Towards understanding deformation and fracture in cementitious lattice materials
Insights from multiscale experiments and simulations

Xu, Yading; Gan, Yidong; Chang, Ze; Wan, Zhi; Schlangen, Erik; Šavija, Branko

DOI
10.1016/j.conbuildmat.2022.128409

Publication date
2022

Document Version
Final published version

Published in
Construction and Building Materials

Construction and Building Materials 345 (2022) 128409

Contents lists available at ScienceDirect

Construction and Building Materials

journal homepage: www.elsevier.com/locate/conbuildmat

Towards understanding deformation and fracture in cementitious lattice materials: Insights from multiscale experiments and simulations

Yading Xu *, Yidong Gan, Ze Chang, Zhi Wan, Erik Schlangen, Branko Šavija

Microlab, Faculty of Civil Engineering and Geosciences, Delft University of Technology, The Netherlands

ARTICLE INFO

Keywords:
Cementitious materials
Lattice materials
Lattice model
Fracture behavior

ABSTRACT

Tailoring lattice structures is a commonly used method to develop lattice materials with desired mechanical properties. However, for cementitious lattice materials, besides the macroscopic lattice structure, the multi-phase microstructure of cement paste may have substantial impact on the mechanical responses. Therefore, this work proposes a multi-scale numerical modelling method to simulate the deformation and fracture behavior of cementitious lattice materials, such that the influence of cement paste microstructure can be properly captured. On the microscale, the load–displacement response of cement paste is numerically simulated then experimentally validated. In order to rationally investigate the role of cement paste microstructure, the obtained load–displacement response was then formulated to several types of model inputs reflecting different degree of brittleness. These inputs were then used for simulating the mechanical response of macroscale cementitious lattices. By comparing the simulation to experiment, multi-linear behavior (ML) was found to an appropriate method to include the realistic pre-critical cracking and post-peak softening of cement paste in the model. Compared to ideally brittle behavior, using ML as input, the discrepancy between simulated and experimentally tested fracture energy decreases from 37.4% to 12.4%. In addition, the influence of lattice structure on the strength of cementitious lattices was also accurately captured by the proposed model. Randomized cementitious lattice has 21.6% (22.0% from simulation) lower strength than regular lattice. Moreover, the influence of fracture criterion of the proposed model is discussed and elaborated. Owning to the high simulation accuracy, the proposed multi-scale method in this work could be helpful for tailoring the fracture cementitious lattice materials for future studies.

1. Introduction

Lattice materials have been widely used in many engineering applications, for instance energy absorption [1–3], sound or thermal insulation [4–6], and catalyst support [7,8]. Over the past decades, numerous types of lattice materials have been created, mainly focusing on using ceramics [9,10], metals [11–14] and polymers [15,16] as the constituent material. In a sharp comparison, although being the most used construction materials, cementitious materials have not attracted enough attention until the most recent years.

3D printing is a commonly used technique to manufacture lattice materials [17–19]. Recently, there has been a rapid development in 3D printing of cementitious materials [20–23]. And gradually, the study of cementitious lattice materials started to attract research interest. The highly porous structure of lattice materials results in significantly lower weight comparing to conventional continuum cementitious materials at the same volume. This feature may give cementitious lattice materials very good thermal insulation properties, similar to the widely used cementitious insulation material: foam concrete. Normally, properties of foam concrete are mainly dictated by the pore structure, which is determined by cementitious mixture proportion. In comparison, besides designing the mixture proportion there is one more dimension of freedom to design cementitious lattice materials by independently designing the lattice structure. Using 3D printing techniques, several studies have already focused on cementitious lattice materials. Aghdasi [24] used a octet type lattice structure to make lightweight cementitious lattice materials. It was indicated by [24] that, when ultra-high performance fiber reinforced concrete was used as the constituent material, the prepared cementitious octet lattice has higher compressive strength than foam concrete with similar porosity. The compressive behavior of octet cementitious lattices was also investigated by [25], in which the tensile resistance of the constituent cementitious material was found to

* Corresponding author.
E-mail address: y.xu-5@tudelft.nl (Y. Xu).

https://doi.org/10.1016/j.conbuildmat.2022.128409
Received 20 April 2022; Received in revised form 15 June 2022; Accepted 4 July 2022
Available online 9 July 2022

play a critical role in determining the compressive strength.

In other studies, [26–28], although not the same lattice structure, tensile stress concentration which led to further cracking was also found to be present on the compressed cementitious lattice materials. This is expected in cementitious lattice materials, due to the quasi-brittleness of the cementitious constituent material. Unlike metals or polymers, the quasi-brittleness makes cementitious materials prone to cracking under tensile stress; in other words, cementitious lattice materials are more defect sensitive. Therefore, in order to study the damage mechanism of cementitious lattices, it is very important to consider the quasi-brittleness induced by the constituent material. In principle, the quasi-brittleness of cementitious materials is induced by the multiple-phase nature of hardened cementitious matrix. Due to the difference in chemical and physical properties of these phases, such as hydrates, anhydrous particles, pores, and air voids, cementitious materials show quasi-brittle fracture behavior. In this sense, reflecting the influence of these compositions would provide in-depth understanding of the fracture behavior of cementitious lattice materials.

In addition to experimental methods, numerical models have been found to be efficient tools to understand mechanical properties of cementitious materials. The lattice type model [29,30] might be a proper tool for simulating the deformation and fracture behavior of cementitious lattice materials. First of all, according to [29,30] the lattice model is able to accurately simulate the deformation and fracture behavior of cementitious materials based on a microstructure-informed approach. As reported in [29], the heterogeneity induced by the multiple-phase microstructure of cementitious materials can be precisely modelled by the lattice model. Moreover, the lattice model may generate a mesh identical to the lattice structure of cementitious lattice materials. This ability not only mitigate potential mesh sensitivity problems which may exist in other type of finite element models, but also provides detailed information of the mechanical response of each individual lattice element. Therefore, the lattice model is adopted here to study the cementitious lattice materials.

In general, this work proposes a multi-scale modeling method to investigate the deformation and fracture behavior of cementitious lattice materials. The lattice model is used to simulate the global tensile fracture process of the cementitious lattices, and local mechanical properties of individual strut elements of the cementitious lattices. With the aid of 3D printing technique, triangular cementitious lattices are prepared and tested under uniaxial tension to validate the proposed method. Based on the experimental and numerical results, a fundamental analysis regarding the role of cement paste microstructure on the deformation and fracture behavior of the cementitious lattice materials is performed.

2. Methods and materials

2.1. Multiscale approach

To provide in-depth knowledge of the deformation and fracture behavior of cementitious lattice materials, a combined experimental and numerical multiscale approach, which was proposed by Qian [29] (from microscale to macroscale) based on the Delft lattice model is adopted here. Schematics of this approach is shown in Fig. 1. The global mechanical response of lattice materials is highly dependent on the mechanical properties of the lattice structure, lattice elements, and the local properties of the constituent material. Therefore, for the studied cementitious lattices, the investigation is also performed on different length-scales, ranging from macroscale global mechanical response of the cementitious lattice material to microscale local properties of hardened cement paste.

On the macroscale, the deformation and fracture behavior of cementitious lattices under uniaxial tension are experimentally and numerically investigated. For cementitious lattice materials, randomized lattice structure may impact the mechanical performance on the macroscale. Therefore, a regular and a randomized lattice structures were used to comparatively study the influence of heterogeneity caused by the lattice structure. Specifically, two triangular cementitious lattices (regular and randomized) are generated, prepared, and tested under uniaxial tension. Schematics of generating the two designed cementitious lattices is shown in Fig. 2. Layer-wise staggered prismatic grids are used to discretize the two-dimensional domain. The vertexes of each grid are aligned on the midpoint of the edge on the previous and the next layer of grids. The length (l) of each grid is 6.0 mm and the height (h) of each grid equals to $\sqrt{3}/2{*}l$. Then, a sub-cell is generated in each grid. The length ($R{*}l$) and height ($R{*}h$) of the sub-cell is proportional to the grid. The length ratio R of the sub-cell to the grid is defined as the randomness of the cementitious lattices. A node is placed in each sub-cell and the struts are generated by connecting nodes in adjacent cells forming a triangular lattice network.

It is worth to be noted that, restricted by inevitable features of cementitious material (to be specific, the shrinkage induced by cement hydration or drying and low tensile/bending strength), dimensions of the prepared specimen are limited. A very large planar plate may result in considerable warping of specimens due to the shrinkage. Therefore, the dimensions of the cementitious lattices are designed as follows (see Fig. 2): the struts of the formed lattice networks are rectangular section

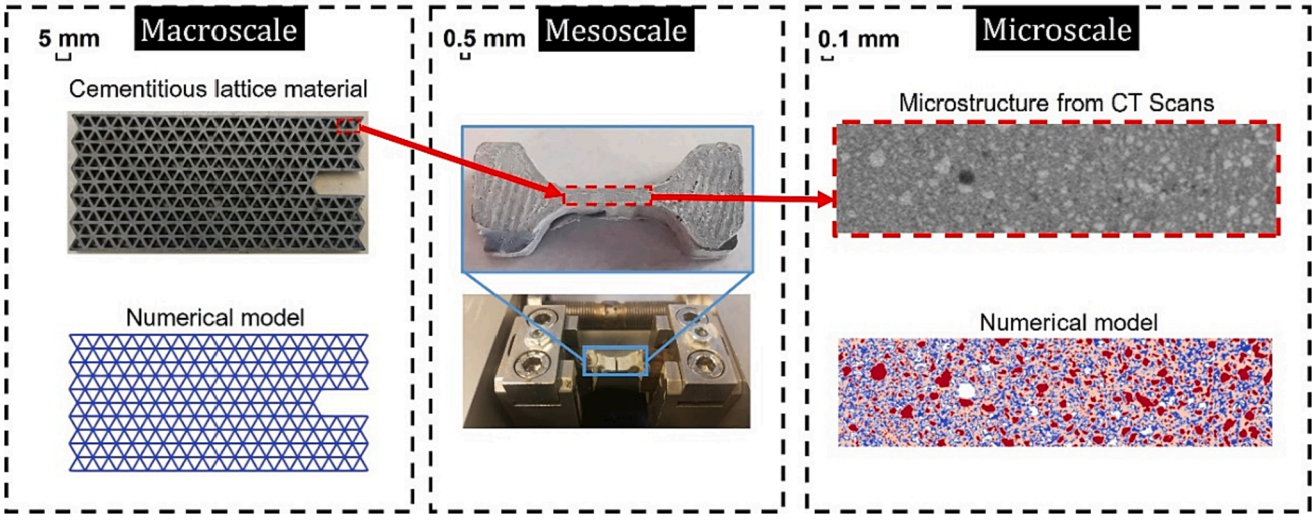

Fig. 1. Schematics of the multiscale approach for studying fracture behavior of cementitious lattices.

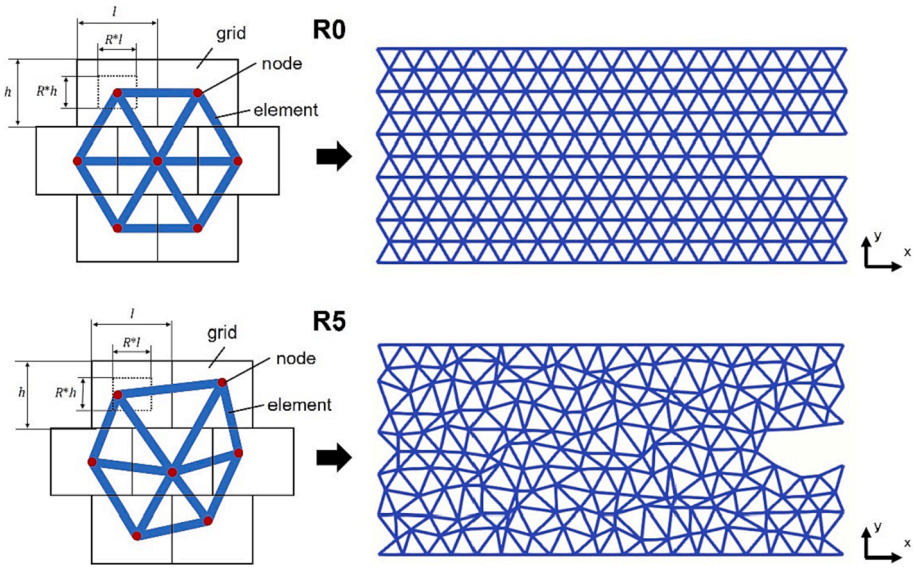

Fig. 2. Schematics of generating macroscale cementitious lattice.

beams with a dimension of 1 × 5 mm (height × depth). The total length, height and thickness of the cementitious lattices are 115 × 53 × 5 mm, respectively. A notch is made by removing 3 × 2 (x axis × y axis) layers of grids on one side of the lattices. Two types of lattices are designed, regular (R0) and randomized (R5). For $R = 0$, the length and height ratio of the sub-cell to the grid equals to 0 and the node is placed at the very center of the sub-cell and the generated lattice network (denoted as R0) is constituted by equilateral triangles; for $R = 5$, the node is placed at a random location within the sub-cell and the generated lattice network (denoted as R5) is constituted by stochastic triangles.

A so-called "in-direct" 3D printing process is used the prepare the cementitious lattices (the sample preparation process is described in Section 2.2), and experimental study is performed using the prepared specimens. Afterwards, numerical models with identical lattice structures are generated to model the deformation and fracture process. In order to obtain input parameters for the numerical model, the mechanical response of lattice element struts is experimentally studied on a lower scale.

On the mesoscale, miniature dog bone shape specimens are used to determine the tensile strength of the cementitious struts by the Micro Tension-Compression Testing stage (Fig. 3). It needs to be noted that as cementitious materials have significant size effect, to validate the simulated strength, it is necessary to use specimens with the same or at least similar size such that the potential influence of size effect can be ignored. The middle part of the dog bone shape specimens is designed to have the same dimension as a single lattice strut used in the macroscale lattice structures. The strain is needed to obtain the E-modulus of the cement struts which will be further used as input for macroscale simulation. However, with the equipment shown in Fig. 3, it is extremely difficult to precisely measure the strain on the small-scale dog bone specimens. Alternatively, the simulated E-modulus from a lower scale (microscale) is adopted for the lattice struts.

On the microscale, the microstructure of hardened cement paste dictates the mechanical properties. In this sense, a micro-structure informed numerical model is used to simulate the tensile stress–strain response of the cementitious struts which forms the macroscale cementitious lattices. The simulated strength is validated by the measured strength of the struts on the mesoscale. As mentioned above, the simulated elastic modulus cannot be validated through mesoscale experimental result because the difficulty of accurately measuring the strain. However, the simulated elastic modulus can be validated by the macroscale experiment and compared to literature data. This is discussed in detail in Section 2.4.2.

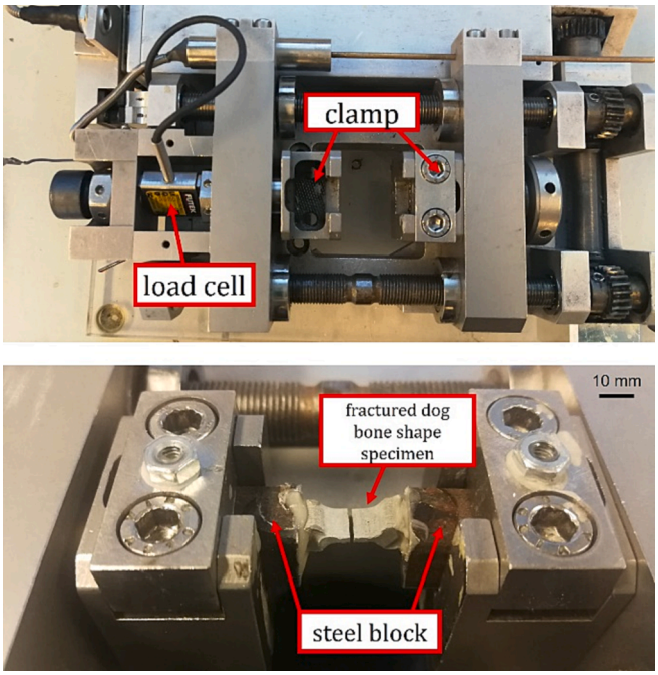

Fig. 3. Micro Tension-Compression Testing stage.

2.2. Specimen preparation

In total, two series of specimens were prepared: cementitious lattice specimens (Fig. 5a) with two different lattice structures to study the global fracture behavior; dog bone shape specimens (Fig. 5b) to obtain tensile strength of the cementitious struts on the mesoscale and the micro-structure of the hardened cement paste which was obtained by CT scan. Dimensions of the dog bone specimen is shown in Fig. 5c.

The specimen preparation method was the same as described in [31]. The procedures are as follows, see Fig. 4:

- A commercial 3D printer (Ultimaker 2 +) was used to print the geometries of the specimens using acrylonitrile butadiene styrene (ABS) as the printing material. The printed mass of ABS for R0 and R5 was 21.3 g and 21.0 g, respectively.

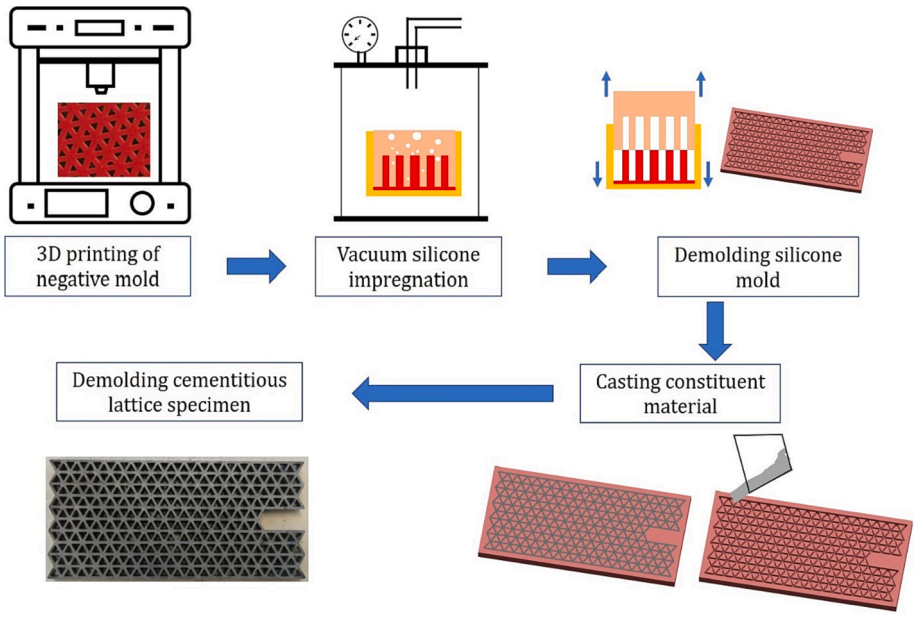

Fig. 4. Specimen preparation procedures.

- The printed structures were glued in a cardboard box. A two-component silicone rubber (Poly-Sil PS 8510) (1:1 by weight) was then vacuum impregnated into the cardboard box (vacuum was kept for 1 min to remove air bubbles). The silicone rubber was left to harden for 2 h in room temperature.
- The hardened silicone rubber was detached from the printed ABS structure, resulting in a mold for creating specimens. These silicone rubber molds are easy to demold and durable enough for reuse.
- Cement pastes with 0.3 w/c (CEM I 42.5 N) were used for casting all specimens. The mix proportion is listed in Table 1. During the mixing process, a Hobart machine was used. All ingredients (cement, water and superplasticizer) were weighted and added to the mixing bowl and then mixed for 4 min. Afterwards, the freshly mixed cement paste was casted into the prepared molds followed by 30 s vibration.
- After 2 days, the specimens were demolded and then cured in water until the age of 14 days.

2.3. Mechanical tests

One hour before testing, the cementitious lattice specimens were surface dried by wiping off water on the specimen surface, painted with white acrylic paint and then sprayed with red dots on the surface in order to enable performing a digital image correlation (DIC) analysis. Uniaxial tensile tests were performed on the cementitious lattices by a hydraulic press INSTRON 8872 with displacement-controlled loading method. As shown in Fig. 6, the displacement is measured and controlled by linear variable differential transducers (LVDTs) at a loading rate of 0.010 μm/s. A schematics of the uniaxial tension test set-up for macroscopic cementitious lattices is shown in Fig. 6. An extremely low loading rate is used here to ensure post-peak behavior of the cementitious lattice can be captured. Uniaxial tensile tests were also performed on the dog bone shape specimens using the Micro Tension-Compression testing stage (shown in Fig. 3) by a displacement-controlled loading rate of 0.10 μm/s, to obtain the tensile strength of the cement paste on the lattice strut scale. The loading rate of the dog bone shape specimens is faster than the cementitious lattices, but still within the quasi-static regime. Therefore, it is assumed that the influence of the loading rate is negligible.

Table 1
Mix proportion of cement paste.

CEMI 42.5 N [g/L]	Water [g/L]	w/c	Superplasticizer (Glenium 51) [g/L]
1616.0	484.8	0.30	2.4

2.4. Numerical simulations

A lattice model was used to perform numerical simulations based on the multiscale simulation framework proposed in [29]. The simulations were performed on two different length-scales: the microscale and the macroscale. As two-dimensional triangular lattice patterns were used to make the cementitious lattice, on both investigated scales, the simulations were also performed using the two-dimensional lattice model.

2.4.1. Theory back ground of the lattice model

As shown in Fig. 7a, in the lattice model a mesh consisting beam elements is used. On the microscale, the mesh is used to discretize a material continuum, namely the cement paste. On the macroscale, the mesh is used to identically represent the triangular lattice structure. The beam elements in the lattice model transfer normal force, shear force and bending moment (see Fig. 7b). Although only 2D triangular patterns were used in this work, spatial 3D beam element is still used in the model. This is consistent with the experimental specimens. Each node of the element has six degrees of freedom: three transitional and three rotational. Detail description of the element stiffness matrix can be found in [29]. To simulate fracture, a prescribed displacement is imposed on the mesh, and a set of linear elastic equations are solved. A fracture criterion (discussed in detail in section 3.3) is given to the lattice element. Base on the fracture criterion, in each step, one element is moved from the lattice mesh such that the fracture process of the lattice mesh is simulated.

2.4.2. Microstructure segmentation

On the microscale, for a given type of cementitious material, the micro-structure is a determinative factor for the mechanical properties. It has been shown by recent studies [32,33] that including the microstructure of cementitious materials in the simulations results in realistic simulated stress–strain response of hardened cementitious materials. In this study, X-ray computational tomography (xCT) was used to obtain the microstructure of hardened cement paste using the dog bone specimen before mechanical test. Grey scale value (GSV) images were obtained from the CT scan at a resolution of 5 μm per voxel. Four phases

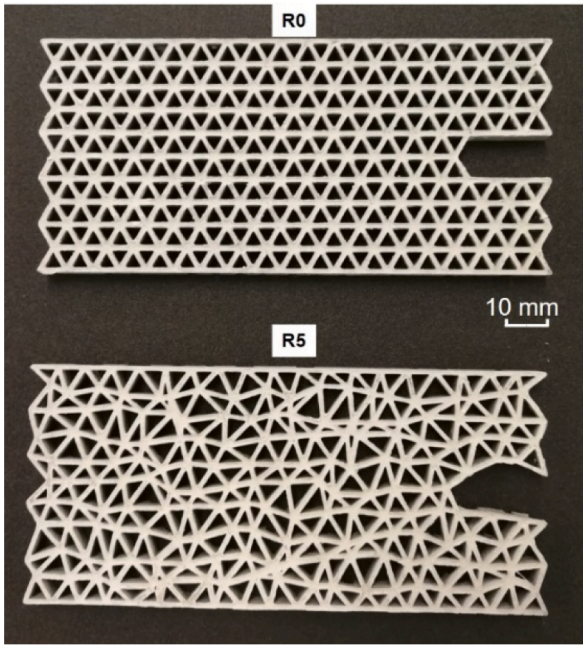

(a)

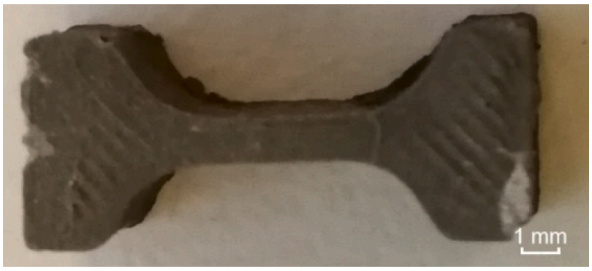

(b)

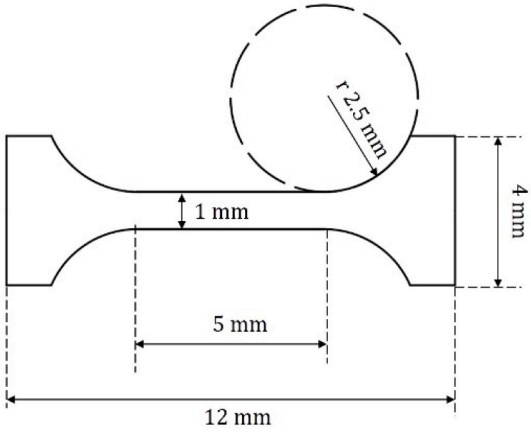

(c)

Fig. 5. Prepared a) cementitious lattice specimen with different randomness, painted in white, b) dog bone shape mesoscale specimen, c) dimensions of the dog bone specimen.

were segmented according to the GSV by the method proposed in [30,34,35]: pores (P), high-density hydrates (H), low-density hydrates (L) and anhydrous cement particles (A). It needs to be noticed, the division of H and L is also based on density, or in other words "porosity". This "porosity" refers to the nanoscale gel pores which does not influence the segmentation of the pore phase (P). The pore phase (P) was first segmented by a threshold (T_1) using the inflection point of the cumulative distribution curve (Fig. 8). Afterwards, anhydrates were segmented using a threshold (T_3) where the derivative of the pixel count curve is approaching zero. After T_3 was determined, the degree of hydration (α) was calculated and an average of 0.61 was obtained. The degree of hydration can be calculated by the following equation [32]:

$$\alpha = \frac{V_{HP}}{\delta_V V_{AH} + V_{HP}} \quad (1)$$

where, V_{HP} is the volume of hydrates; δ_V is a constant determined by cement compositions which is typically 2.2;V_{AH} is the volume of anhydrates.

At last, the volumetric ratio of low-density hydrates (V_L) to high-density hydrates (V_H) was determined. According to the results reported in [36], the ratio of V_L to V_H is directly related to the degree of hydration. For cement paste with a w/c = 0.3, the volumetric ratio V_L/V_H is within a relatively narrow range between 0.65 and 0.81, as long as the degree of hydration α exceeds 0.4 [36]. Therefore, 0.75 is assumed as the overall V_L/V_H value within all tested images thus a fixed T_2 was obtained. In total, four phases were segmented, details are given in section 3.

2.4.3. Lattice network generation

On the macroscale, the lattice networks were kept identical to the lattice structure of the experimental specimens (R0 and R5, respectively).

On the microscale, lattice networks were generated based on the segmented GSV images from X-ray tomography images. A domain covering 200 × 800 pixels on the GSV picture was first generated. A node was placed in the center of each pixel (except the pore phase) and lattice elements were generated by connecting adjacent nodes forming a triangular lattice network. The heterogeneity of the hardened cement paste was introduced to the generated lattice network by mapping local mechanical properties of these segmented phases according to their GSV values. Therefore, in total of six types of elements were generated. Elements with both nodes locating in the pixels of the same phase were assigned with mechanical properties of the corresponding phase. Elements with nodes located in the pixels of two different phases were identified as interface elements between the two phases, and they were assigned with arithmetic averaged mechanical properties of the two corresponding phases. The schematics of generating lattice network based on the GSV pictures is shown in Fig. 9.

2.4.4. Lattice fracture modeling

After the lattice network was generated, mechanical properties of each segmented phase were assigned to the corresponding phase. Then, a set of linear elastic analyses was performed under a uniform prescribed displacement imposed on the right-side boundary of the generated lattice system, while the left-side boundary was clamped (Fig. 1 left). Elements on the boundary layers were prohibited from failure in order to maintain the path of force transferring. In each step the stress on each element was calculated, and one element is removed from the lattice system as long as it violates the fracture criterion. The fracture criterion of the model is discussed in detail in section 3.3.

On the microscale, as each element represents a relatively small region of material (5 μm), it was not possible to experimentally detect the softening behavior of the phases in hardened cement paste. Similar to many other studies [37–39], the mechanical behavior of these phases on this scale is assumed as linear-elastic perfectly brittle, namely the stress linearly increases with strain before tensile strength and no strain

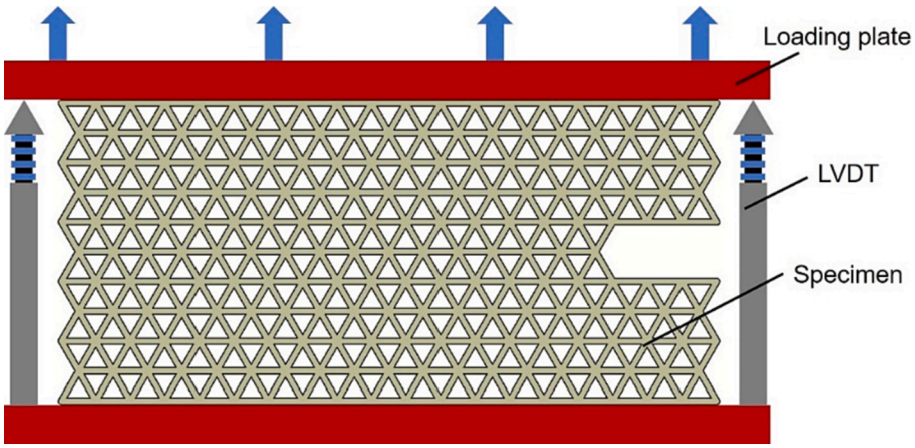

Fig. 6. Schematics of uniaxial tension test set-up for macroscopic cementitious lattices.

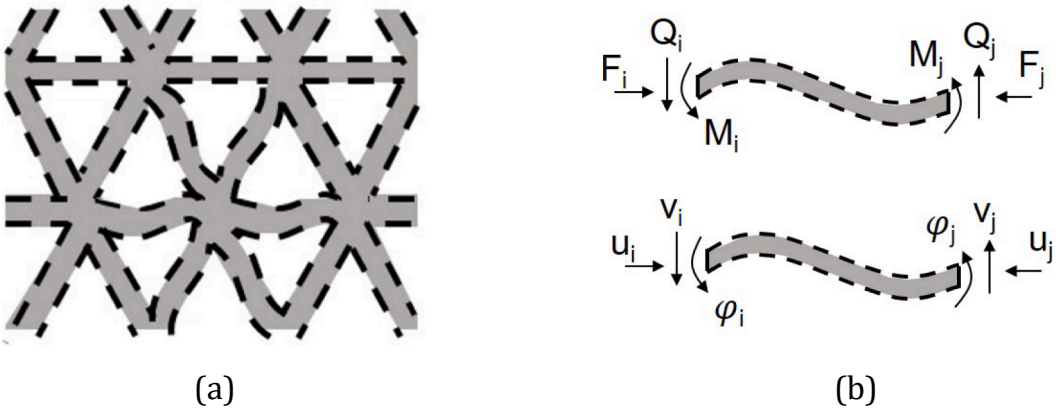

Fig. 7. Schematics of a) triangular lattice mesh consists beam elements; b) forces and deformation on a single element.

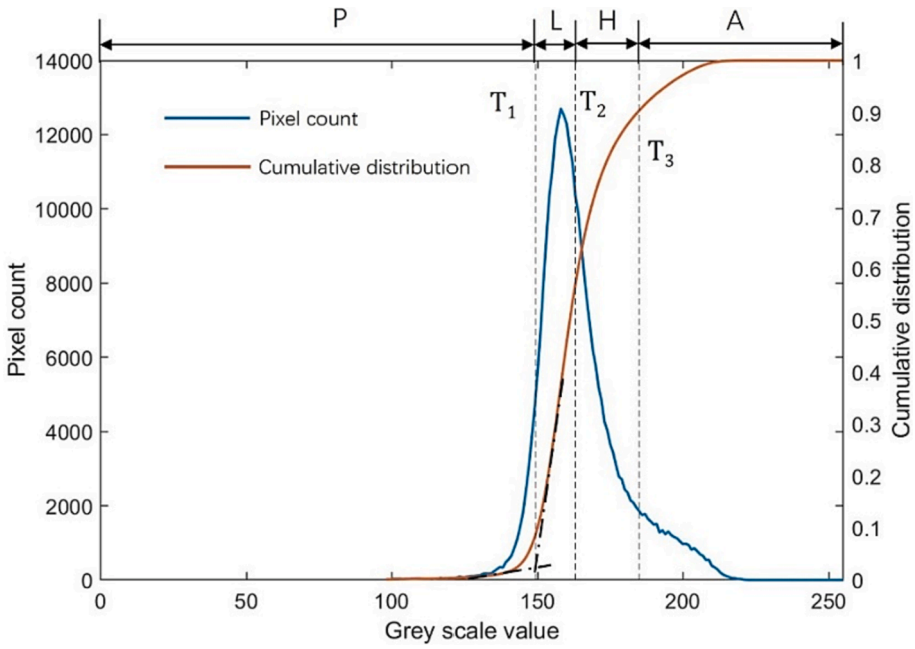

Fig. 8. Phase segmentation based on grey scale value histogram.

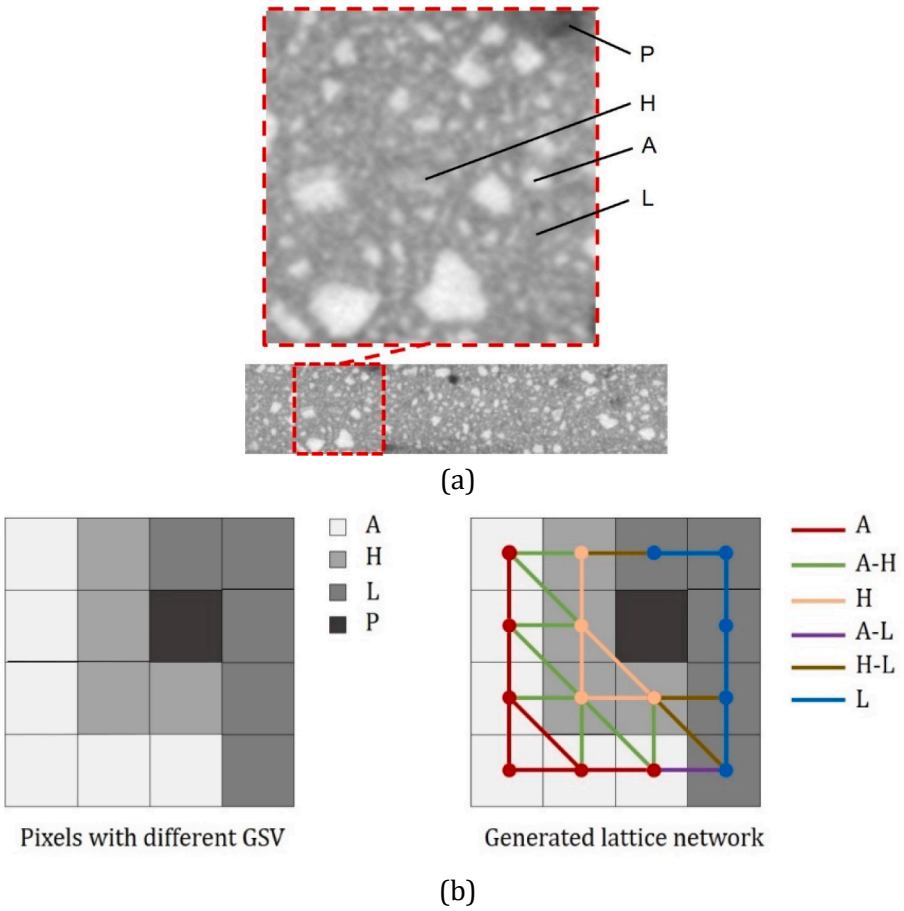

Fig. 9. Schematics of a) GSV picture from CT scan with different phases, b) generating lattice network based on the phases segmented from GSV picture, anhydrous cement particles (A), high-density hydrates (H), low-density hydrates (L), pores (P) and their interface phases are indicated.

softening is present after the peak load. Input mechanical properties of the segmented phases are based on the previous studies of the authors and listed in Table 2. The E-modulus and tensile strength of the low-density hydrates (L), high-density hydrates (H) and anhydrates (A) were adopted according to the curing time, referring to literatures [30,37] in which the mechanical properties of these phases were tested on a scale similar to this study.

The results from microscale simulations were used as the struts input properties for the macroscale modelling of the cementitious lattices. It was indicated in [15] that the local pre-critical cracking (the stress–-strain branch between elastic stage and peak strength) or softening behavior of polymeric lattice struts in numerical models have significant impact on the fracture behavior of lattice materials. For the lattices in this work, the cementitious struts may also exhibit local pre-critical cracking and softening because of the heterogeneous microstructure of hardened cement paste. Therefore, in order to investigate the influence of microscale heterogeneity, three types of constitutive behaviors were used as the struts input properties based on the struts stress–strain response obtained from microscale simulations. These three types of constitutive behavior represent gradually increased heterogeneity. Schematics of the three types of behavior is shown in Fig. 10:

- Single linear (SL) behavior, which corresponds to an ideally-brittle response of homogeneous material, namely only the strut deforms elastically and fails immediately when its strength is reached. E-modulus corresponds to the elastic branch and strength equals to the tensile strength.
- Bi-linear (BL) behavior, which indicates the strut has slightly increased heterogeneity comparing to the SL. Two linear pre-peak segments were used such that the pre-critical cracking is included.
- Multi-linear behavior (ML), in which five linear segments were used: the elastic branch; the peak stress; and 70%, 40% and 20% of the peak stress in the post-peak regime, such that pre-critical cracking and softening are all included.

In the simulation, a strut with SL behavior is immediately removed from the lattice system when the peak stress is reached. While struts with BL and SL behavior lose their strength and stiffness gradually (following the input constitutive behavior in steps), until eventually being removed from the lattice system through several analysis steps. Note that, considering the brittleness of cement paste, no plasticity effect is considered. For all three types of inputs, the linear behavior always discharges at zero.

Table 2
Input parameters of the segmented phase on the microscale, partially from [30,37].

Phases	E (GPa)	G (GPa)	f_t (MPa)	f_c (MPa)
L	21.6	9.0	55.0	$-f_t$ *8
L-H	26.4	11.0	65.0	$-f_t$ *8
H	31.2	13.0	75.0	$-f_t$ *8
L-A	58.4	24.3	35.3	$-f_t$ *8
H-A	63.2	26.3	36.3	$-f_t$ *8
A	95.2	39.6	650.0	$-f_t$ *8

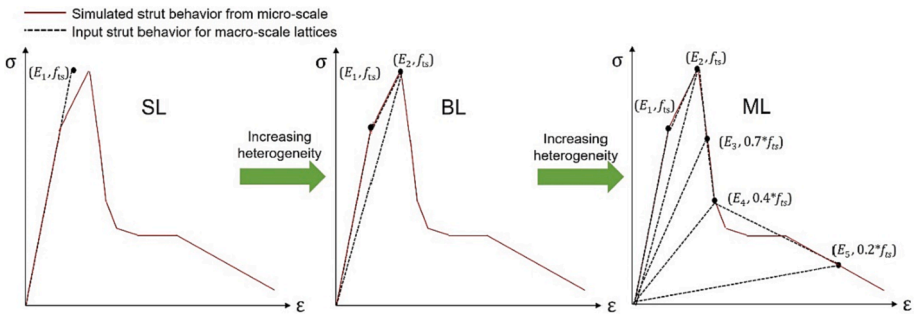

Fig. 10. Schematics of stress–strain curve obtained from microscale simulation and the corresponding strut input behavior for macroscale cementitious lattice.

3. Discussion

3.1. Mechanical properties of cementitious struts

Quasi-brittle tensile behavior is commonly seen in hardened cement paste, i,e, a softening branch can be found in the stress–strain response. As described in Section 2.4.4, to simulate the fracture behavior of the macroscopic cementitious lattices, a proper stress–strain response of the cementitious struts was needed. Limited by the experimental set-up, it was not possible to experimentally determine the entire stress–strain response (especially the softening branch) of the cementitious struts on the mesoscale. Therefore, it was necessary to numerically simulate the stress–strain response of the cementitious struts on a lower scale (microscale) such that the stress–strain response of the struts can be obtained.

On the microscale, hardened cement paste is typically seen as heterogeneous due to the complex chemical composition of different phases and their spatial distribution. In this sense, it is important to properly segment the microstructure of hardened cement paste. Using the GSV based method, different phases were segmented. For the studied cases, in total 20 GSV images were used, and a volumetric ratio of the segmented phases in these specimens is shown in Fig. 11. On average, the degree of hydration of these specimens is 0.61 ± 0.04 and the ratio of the low-density hydrates to high-density hydrates V_L/V_H is 0.75 ± 0.16. These values are consistent with the results in the literature [32,36,40,41], which ensures the accuracy of the simulations later. Comparison of a GSV picture and the segmented phases is shown in Fig. 1.

Typical simulated stress–strain responses of the lattice struts are shown in Fig. 12, for conciseness only 10 results are shown. After the elastic stage, the strut did not fracture immediately, so, a short pre-critical crack branch (from point "1″ to point "2" in Fig. 12) [42] can be found before the tensile strength. Therefore, for the macroscopic cementitious lattice simulations, if the behavior of a strut is assumed to be pure brittle (SL), the E-modulus should be equal to the slope of the curve calculated at end of the elastic stage (point No.1 in Fig. 12), while the stress equals to the ultimate tensile fracture strength (point No.2 in Fig. 12) of the strut (see Fig. 10a).

As describe before, the strength of the cementitious struts was experimentally measured. A comparison between the simulated and experimentally measured tensile strength of the struts is shown in Fig. 13. The microscale simulation results agree with the experiments well, not only in terms of the average strength, but also in terms of the standard deviation induced by the high heterogeneity of microscopic cement paste. In this sense, the microscale simulations can be considered as experimentally validated.

The large deviations observed both from experiment and simulation indicate that the heterogeneity of the lattice struts should not be neglected when studying the macroscale cementitious lattices. Therefore, to properly simulate the mechanical response of the macroscale cementitious lattices, using the average value as the input for the struts in the macroscale lattices is not the best choice. Instead, using randomly selected values (obtained from microscale simulations) allows considering the influence of microscale heterogeneity on the mechanical response of macroscopic cementitious lattices.

After reaching the tensile strength (No.2 in Fig. 2), as expected, the struts show an obvious tensile softening behavior. Correspondingly, a tortuous crack pattern can be observed during the fracture process of the

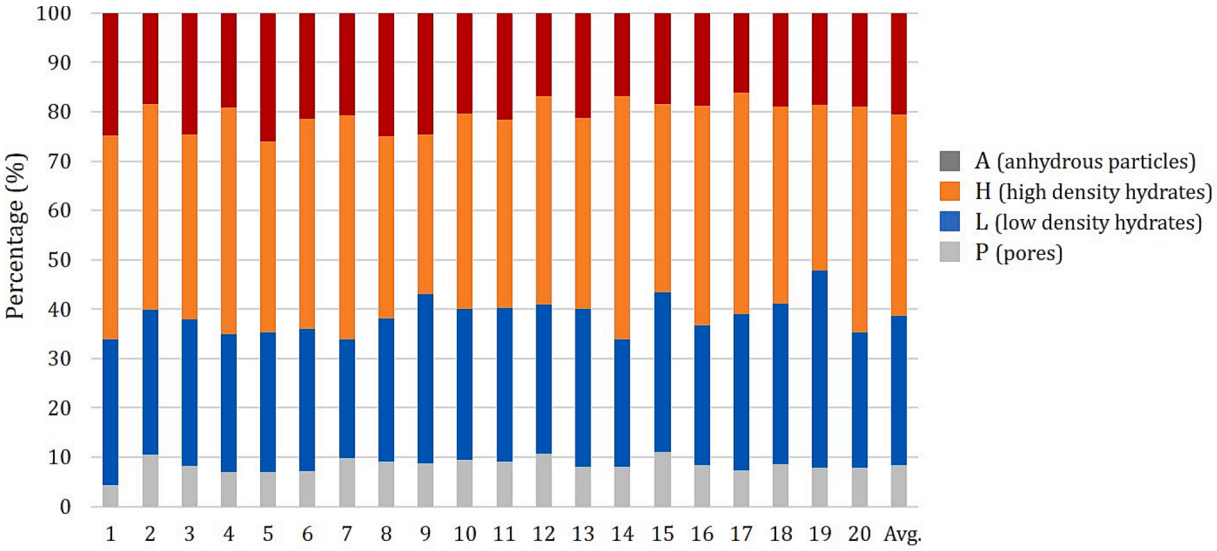

Fig. 11. Volumetric ratio of four segmented phase in all obtained GSV images, horizontal axis indicates image number.

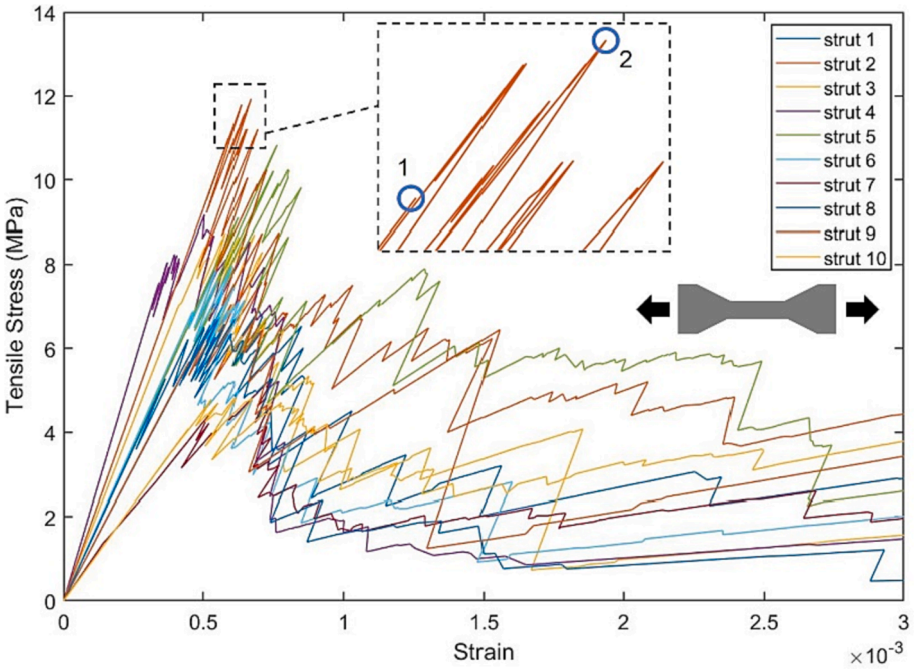

Fig. 12. Simulated stress–strain responses of the cementitious struts, for conciseness only 10 results are shown; point No.1 indicates the end of the elastic stage where the first lattice element is damaged; point No.2 indicates the tensile fracture strength of the strut.

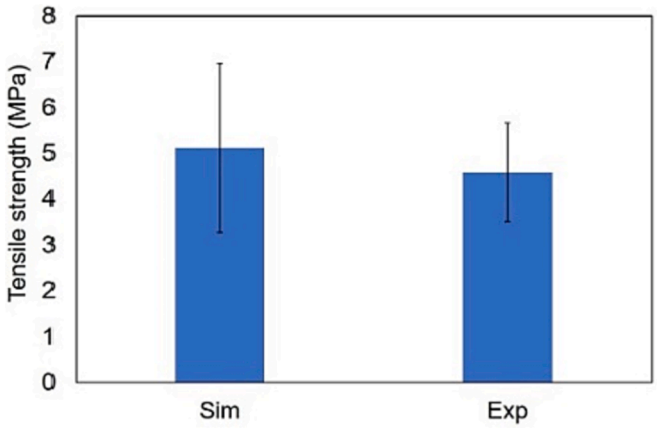

Fig. 13. Tensile strength of the cementitious strut obtained from mesoscale experiment (obtained from dog bone shape specimens) and simulations; standard deviation is indicated by the error bars.

cement struts. From the crack pattern (indicated in black in Fig. 14), it is clear that the pores played a critical role: cracking initiated at locations with high local porosity; then propagated through the weaker phase (L, low density hydrates); eventually a tortuous main crack was generated. In addition, the distributed cracks locating outside the main cracking plane also contributed to the overall softening behavior, therefore, an obvious softening branch can be found in the stress–strain curve of cement struts in Fig. 12.

3.2. The role of microscale heterogeneity of cement paste

The microscale heterogeneity is an intrinsic feature of cementitious materials. This is mainly determined by the multi-phase nature of hardened cement paste, which has already been discussed in section 3.1. In this work, the influence of microscale heterogeneity on the mechanical properties of cementitious lattices mainly exists in the pre-critical cracking branch (the curve between first cracking point to the peak load point of each curve, see Fig. 15). Although using all the three strut behaviors (SL, BL and ML) as input the load–displacement response of cementitious lattices can be roughly captured by the simulated curves, the long pre-critical cracking branch can be only found on the curves simulated with the quasi-brittle strut behavior (BL and ML). While for the SL, the pre-critical cracking branch is much less visible. The existence of pre-critical branch is an important indicator of the quasi-brittle fracture behavior of the cementitious lattice, and this will be discussed in detail later.

For the studied quasi-brittle fracture process, it can be assumed that the total work applied on the cementitious lattice comprises by three parts, as shown in Fig. 16: elastic energy (E_e), pre-critical cracking energy (E_p) and post-peak cracking energy (E_c). The fracture energy (E_g) is defined as the sum of the pre-critical cracking energy (E_p) and post-peak cracking energy (E_c). Note that within the pre-critical cracking branch and the post-peak branch, there was also some energy dissipated by sound or heat which are also included as the fracture energy here. As described previously, during the computing process, the lattice model gives load–displacement curves with true snapbacks (see Fig. 15). However, this was not captured in the experiment performed in this work, as the upper and lower boundary of the cementitious lattices were loaded under a constantly increasing displacement. To ensure a precise fracture energy calculation, the simulated load–displacement curves were also smoothed (see Fig. 15 the colored dash lines) such that the displacement of the simulated curves monotonically increases which corresponds to the experiment condition.

Fig. 17 shows the total work and fracture energy of the cementitious lattices. If only considering the total work, it seems that the microscale heterogeneity doesn't significantly influence the fracture of cementitious lattices because using any of the three types of strut behavior the model obtained similar simulation results which show good agreement with experiment (the BL is only higher by 11% comparing to experiment). However, solely examining the total work doesn't properly reflect the real fracture behavior of the cementitious lattices. From the fracture energy point of view, the determinative role of the microscale heterogeneity can be identified. As can be seen from Fig. 17, the simulated fracture energy of SL is 37.4% lower than the experiment, which is mainly caused by the ignorance of the pre-critical cracking and post-

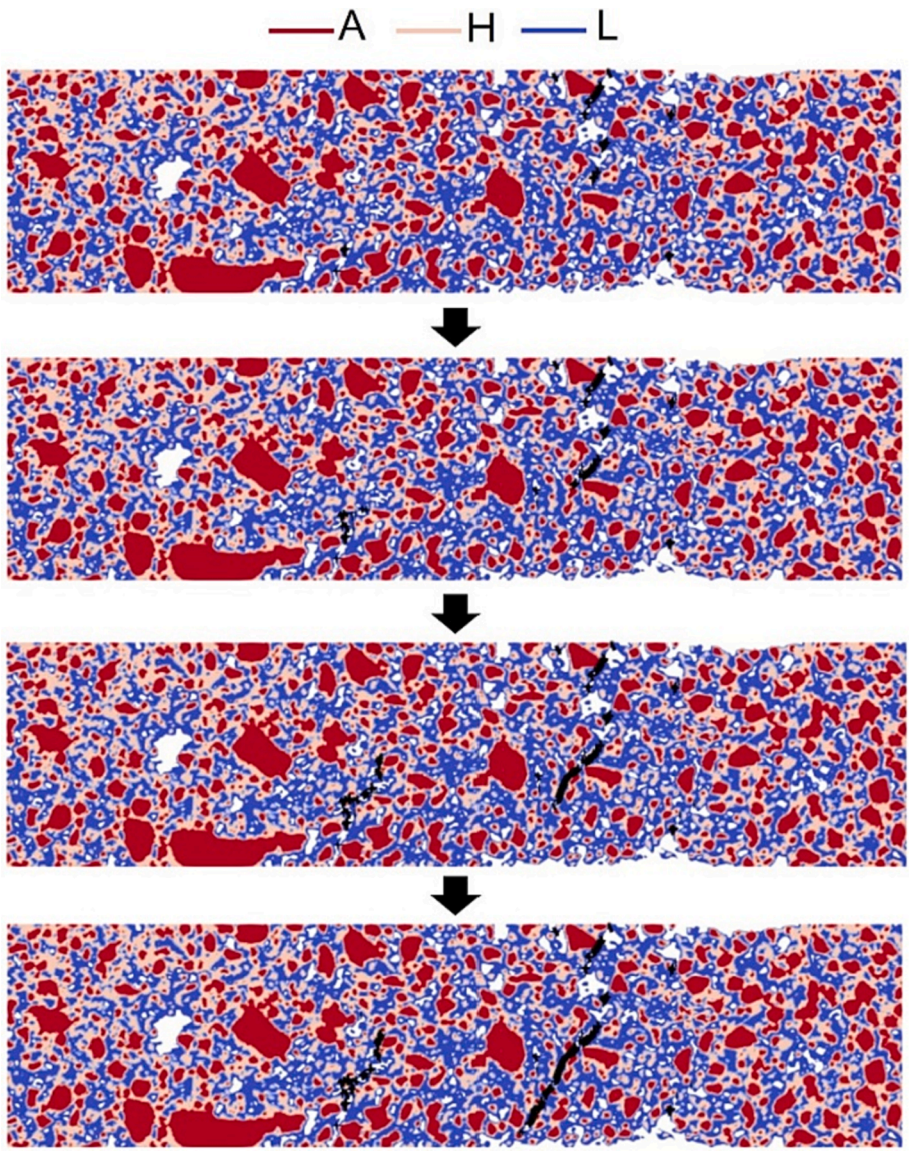

Fig. 14. Simulated crack pattern of the cementitious struts, failed elements are indicated in black; anhydrous particles (A) are indicated in red; high-density hydrates (H) are indicated in pink; low-density hydrates (L) are indicated in blue; white areas are pores; the quantities of the interface elements are too small to be visible.

peak softening of the cementitious struts. Increasing the heterogeneity by including the pre-critical cracking, the BL shows better agreement with experiment which is 20.7% higher than experiment value. Furthermore, when the post-peak softening is also considered, the ML is only 12.4% higher that the experiment. In this sense, the microscale heterogeneity crucially determines the fracture energy of cementitious lattices.

Still, in general the simulated fracture energy values are on average higher than experiment. This was mainly caused by the lower simulated stiffness (see Fig. 19) of the lattices such that more energy was left when the elastic energy was excluded from the total work.

3.3. Mechanical properties of cementitious lattice with varied lattice structure

Now that the ML is proven to be an appropriate model input for macroscale simulations, it would be possible to predict the mechanical response of cementitious lattices with different lattice structure. As mentioned previously, cementitious lattice with a randomized lattice structure (R5) was also prepared. As can be seen from Fig. 18, in general using ML the simulation also shows good agreement with the experiment on R5. Moreover, it has been reported that the stiffness of triangular lattice is relatively insensitive to the nodal randomness [43]. Similar result is also found for the studied cementitious lattices. It can be seen from Fig. 19 that the simulation results show reasonable agreement with the experiment, both for R0 and R5. No significant difference between the stiffness of regular lattice (R0) and randomized lattice (R5) can be observed from the experimentally and numerically obtained results. It's worth noticing that, for both R0 and R5, the simulated stiffness values are lower than the experimental values. This is possibly caused by the so-called "joint stiffening" effect. As shown in Fig. 20, the joints between the lattice struts in experiment also account for a certain amount of material. Besides the elements, this joints also bears load and contribute to the global stiffness of the cementitious lattice [44,45]. In contrast, in the simulations, the lattice elements were only connected at the node. The numerical node can be regarded as a point without volume, therefore, don't bear extra load as the joint do. For further studies, this "joint stiffening" effect may be compensated by increasing the size of elemental cross section.

Comparing to the stiffness, the tensile strength of cementitious lattices is found to be more sensitive to lattice structure. Fig. 19 clearly shows that the tensile strength of the regular cementitious lattice (R0) is

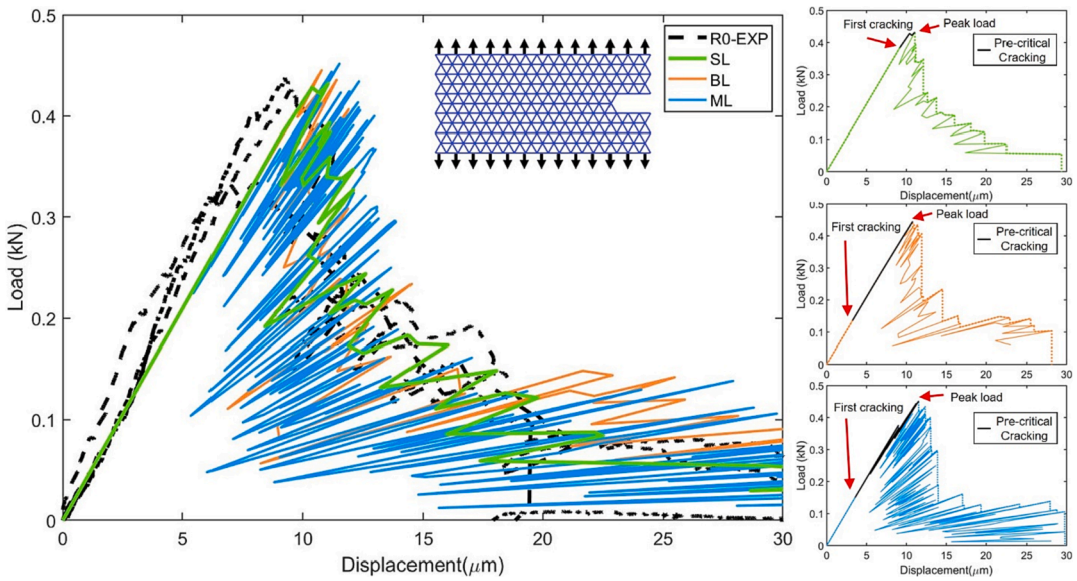

Fig. 15. Load-displacement curves of R0 obtained from experiments and simulations using different struts behavior as model input; the dashed color lines are the smoothed curve of the simulation results.

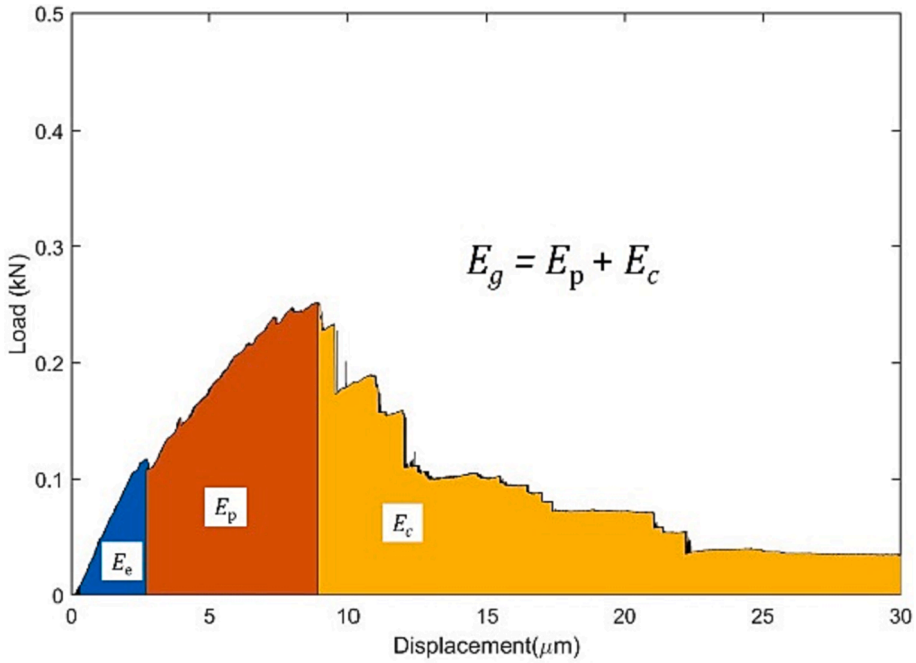

Fig. 16. Energy components during fracture process of cementitious lattices.

21.6% (22.0% from simulation) higher than the randomized cementitious lattice (R5). Correspondingly, the simulation also captured this phenomenon. Furthermore, the simulated tensile strength values are higher than those obtained from experiments. One reason could be attributed to the local defects of the macroscale lattices, namely the sharp corners in the vicinity of the joints, as shown in Fig. 20. These sharp corners may introduce extra stress concentrations on the lattice struts thus the struts in the experiments may break before the simulated critical stress was reached. This extra stress, however, can't be accounted for in the simulations. A similar effect introduced by the joint of lattice struts was also found in [15]. It was shown in Fig. 13 that the simulated strut strength is slightly higher than the experimental values, this may also contribute to the higher simulated strength of the cementitious lattices.

In summary, using the ML as input, the multi-scale model also gives accurate simulation results when a different lattice structure (R5) is used. This indicates that the prosed modeling method has great potential to help design cementitious lattice materials with tailored mechanical properties.

3.4. Discussion of the fracture criterion

As mentioned previously, in the lattice model the fracture process is simulated by sequentially removing failed elements from the lattice system. Therefore, the breaking law (fracture criterion) of the beam elements need to be carefully determined to obtain more accurate simulation result. In previous studies [46,47], a simple fracture criterion was proposed, written as Eq. (2). When the effective stress σ exceeds the

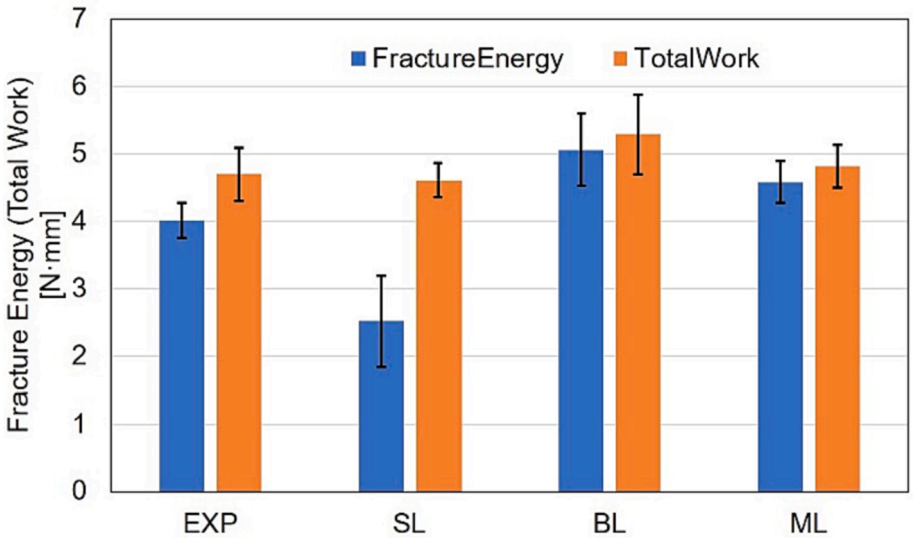

Fig. 17. Fracture energy and total work of the cementitious lattices obtained from experiment and simulations, standard deviation is indicated by the error bars.

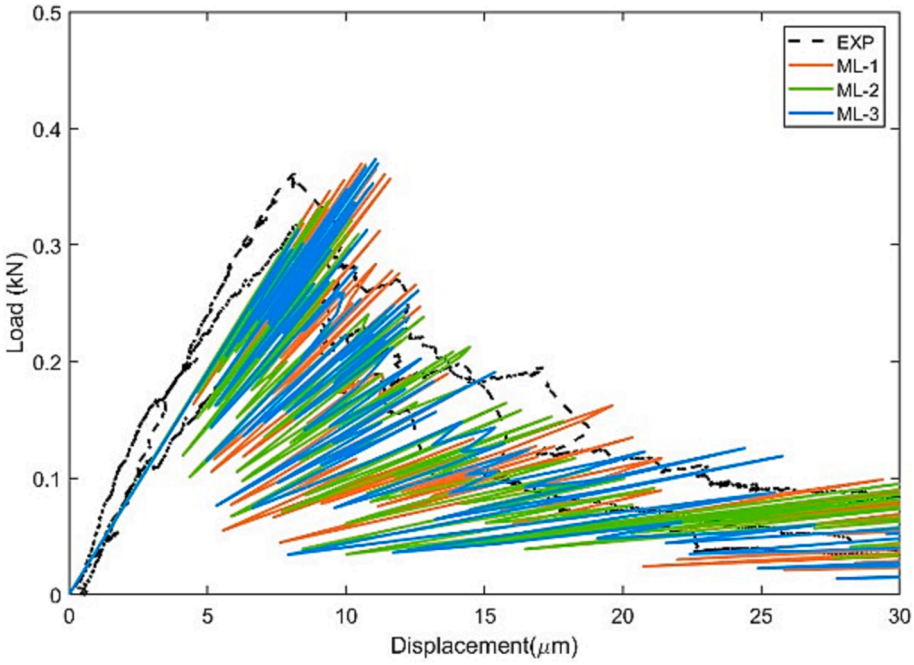

Fig. 18. Simulated load–displacement curves of R5 using ML as input, the simulation is repeated for three times in total.

tensile strength of the beam, the element will be removed from the lattice.

$$\sigma = \frac{N}{A_s} + \alpha_M \frac{max\left(|M_i|, |M_j|\right)}{W} \tag{2}$$

Where, N and A_s is the normal force and the cross-sectional area of the beam element; M_i and M_j are the bending moments in the nodes i and j of the beam element; W is the cross-sectional modulus of the beam element; α_M is the coefficient that regulates the contribution of bending moment on the effective stress on the beam. The choice of α_M may have an obvious influence on the fracture process of lattice network and it may vary with different lattice models. The determination of α_M is, then, critical. According to previous studies [29,47,48], depending on the lattice network structure, different α_M values were used, ranging from 0 to 1. Similarly, this range is also adopted here to study the influence of α_M.

3.4.1. *Cementitious struts*

For the simulation of the cementitious struts, the coefficient α_M mainly influences the simulated tensile strength and crack pattern. On one hand, according to eq.2, α_M indicates the amount of bending moment used to calculate element stress. When $\alpha_M = 0$ is adopted, the bending moment is completely ignored, as a result, beam elements would fail only if the tensile stress induced by normal force exceeds the tensile strength. Then, the simulated struts will show relatively higher strength than any other cases with $\alpha_M > 0$. It can be seen from Fig. 21a that, the simulated strength for $\alpha_M = 0$ is approximately 10 MPa which is strikingly higher than the experimentally measured cement struts strength (approximately 4 MPa ~ 5 MPa as indicated in Fig. 13). Increasing α_M from 0, an increasing fraction of bending moment starts to be taken into consideration, consequently the simulated tensile strength of cementitious struts also decreases. Ultimately, when $\alpha_M = 1$ is used, both normal force and bending moment are entirely included to

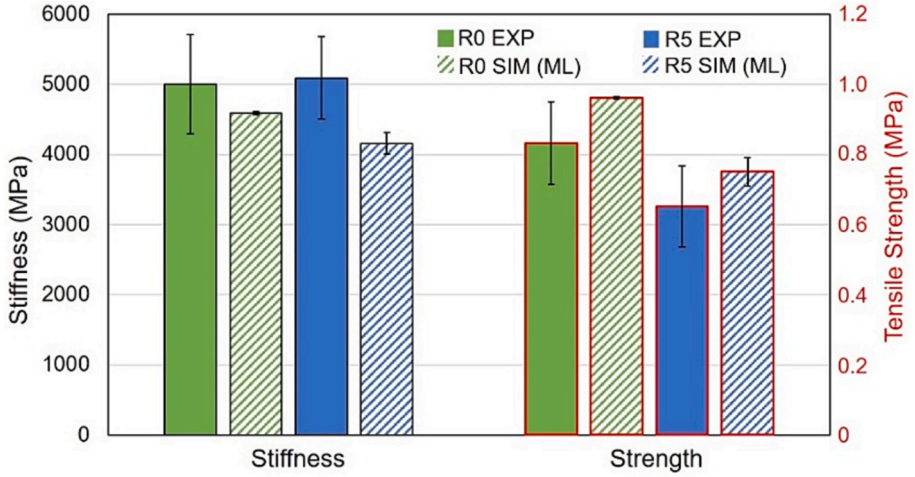

Fig. 19. Comparison of the stiffness and strength of the cementitious lattices with different randomness, standard deviation is indicated by the error bars.

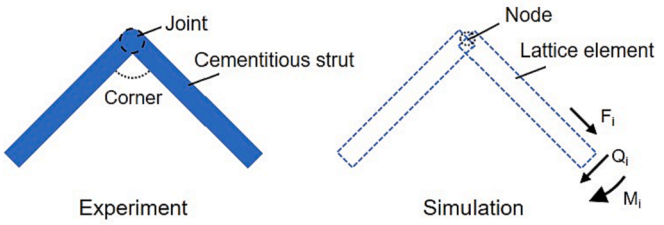

Fig. 20. Schematics of the comparison between connected beams in the experiment and simulation.

calculate the tensile stress on the lattice beam elements, therefore, the lowest strut strength is obtained.

On the other hand, the simulated crack pattern is also dictated by the parameter α_M. For the numerical lattice network used in this work (shown in Fig. 9), it is obvious that under uniaxial tensile load horizontal lattice elements bear lower normal force than any other elements, because they are perpendicular to the loading direction. When a small value (for instance $\alpha_M = 0$ and $\alpha_M = 0.05$) is assigned to α_M, it is the normal force that determines the tensile stress on the elements. As a result, the simulated tensile stress on these horizontal elements is the lowest among all elements. Then the horizontal elements are more unlikely to fail comparing to other elements. Eventually, the main cracking plane formed a transverse pattern across the strut, mostly consisting vertical and diagonal elements (as can be seen from Fig. 21b). Increasing α_M, the influence of bending moment on element stress starts to emerge and becomes more and more obvious, this means that the tensile stress on the horizontal elements can be higher than other elements. As a result, it can be found in Fig. 21b that many horizontal elements also failed allowing the cracking plane propagated to the diagonal direction when $\alpha_M = 0.5$ and $\alpha_M = 1$ is adopted.

What has to be mentioned is that, for the cementitious struts, the lattice system is only used to model the mechanical behavior of cement paste instead of constructing the real microstructure. In the numerical model, a continuum material is discretized by lattice beam elements. This means that these elements do not physically exist but virtually represent the mechanical response of different phases and the interaction between these phases. Therefore, the α_M is only a tunable parameter of the lattice model not a physical constant with accurate definition. Then, the choice of α_M only need to follow a consequential approach. For the used four different values, $\alpha_M = 0.5$ gives the best agreement with experiment in terms of tensile strength. So, it's used for all simulations for cementitious struts.

3.4.2. *Cementitious lattices*

Different from the microscale simulations, the macroscale numerical lattices directly represent the experimental specimens, because of the numerical models and experimental specimens have identical lattice structure. Therefore, the coefficient α_M should be chosen such that the stress distribution on a beam under tensile and flexural load can be correctly reflected, namely in theory $\alpha_M = 1$ should be used. However, as shown in Fig. 22, when $\alpha_M = 1$ is used the simulated load–displacement responses of the cementitious lattices are obviously more brittle than experiments, especially for R0. This discrepancy is assumed to be caused by the presence of the joints connecting cementitious struts. Comparing to the numerical struts under the same bending moment, higher stress might be present on the cementitious struts during experiment due to potential joint-stiffening effect. Therefore, for the macroscale lattice model, a smaller value needs to be given to the coefficient α_M as a compensation of the joint-stiffening effect.

As shown in Fig. 22, decreasing α_M doesn't significantly influence the strength of cementitious lattices. The influence of α_M mainly exists in the post-peak branch of the simulated load–displacement responses. When $\alpha_M < 0$ is used, indeed the simulated load–displacement curves correspond better with experiment, and the simulated curves agrees with experiment very well either $\alpha_M = 0.05$ or $\alpha_M = 0$ is used. Nevertheless, when $\alpha_M = 0$ is adopted, the failed elements are almost at the diagonal direction, and the cracking is deflected near the notch forming a branched main crack. This behavior obviously deviates from the DIC results (as shown in Fig. 23) obtained from experiment. In this sense, $\alpha_M = 0.05$ is the best choice among all these simulation cases, therefore, it was used for all the simulations for macroscale lattices.

The influence of α_M on the post-peak behavior is caused by the element orientation-dependent fracture feature of the lattice model: when smaller α_M is used, the tensile stress on horizontal elements is also smaller than other elements because less bending moment is included; so, the horizontal elements are less likely to fail under uniaxial tension and it is more difficult to form a main cracking plane; therefore, less brittle response would be obtained.

Similarly, the influence of α_M on the post-peak behavior can be also found for the heterogeneous cementitious lattice R5. As can be seen from Fig. 23, the cracking plane observed in the experiment is rather tortuous. Correspondingly, a tortuous main cracking plane can also be found in the simulated crack pattern either $\alpha_M = 0$, $\alpha_M = 0.05$ or $\alpha_M = 0.5$ is used (see Fig. 22b). When $\alpha_M = 1$ is adopted, a relatively straight transverse main cracking plane can be observed, and correspondingly more brittle load–displacement response is found. While, the sharp difference found in R0 between $\alpha_M = 0$, $\alpha_M = 0.05$ is not visible for R5. This indicates that the orientation-dependent fracture behavior found in

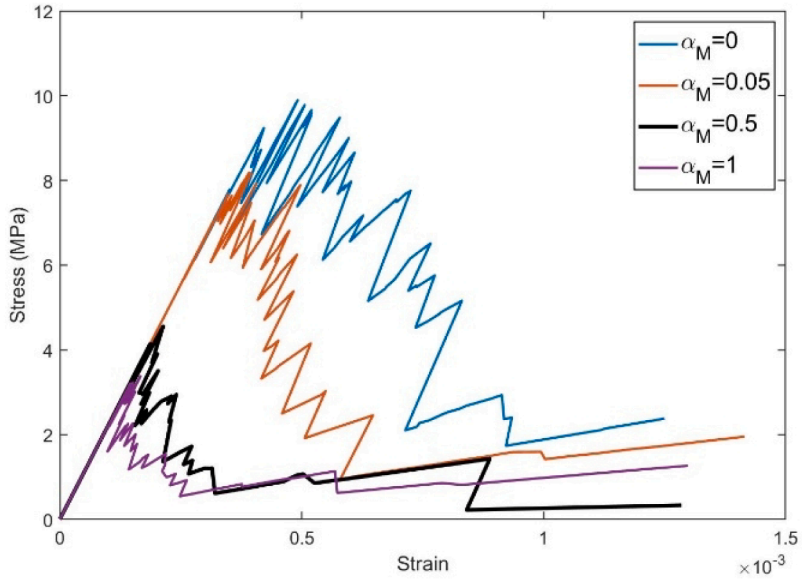

(a)

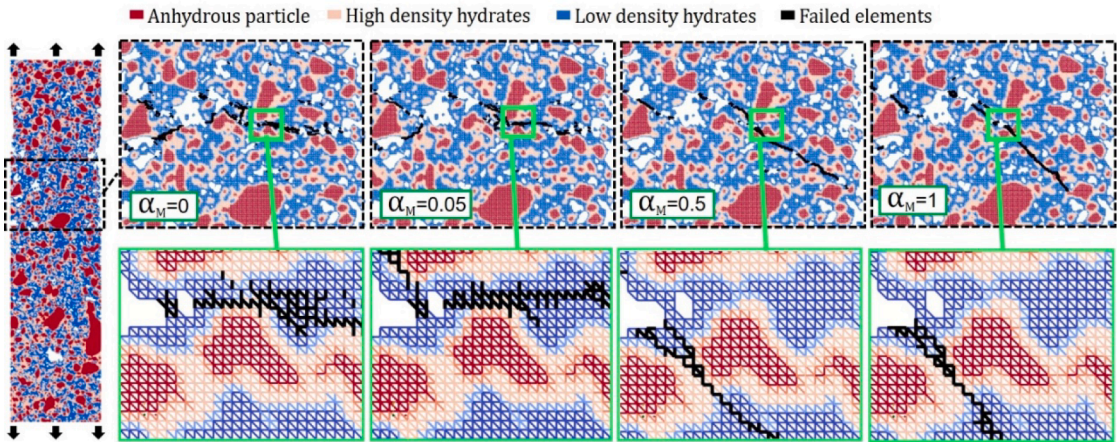

(b)

Fig. 21. Simulated a) stress–strain curves of a cement strut using different coefficient α_M; b) fracture pattern of the cement strut.

regular cementitious lattice is mitigated by the randomized lattice structure. In general, for both R0 and R5, using $\alpha_M = 0.05$ the simulations show the best agreement with experiment.

4. Conclusions

In this work, a coupled experimental-and-numerical investigation focusing on the deformation and fracture behavior of cementitious lattice materials is presented. An experimentally validated multi-scale modeling method is proposed to predict the mechanical response of cementitious lattice materials. In addition, the fracture criterion of the proposed multiscale lattice models is also discussed. Based on the obtained results, several conclusions can be drawn as follows:

- The proposed multi-scale lattice model is proved to be able to accurately simulate the fracture behavior of cementitious lattice materials. It is found that the using multi-linear behavior (ML) as input, the realistic pre-critical cracking and post-peak softening of cement paste can be properly considered in the model. Compared to ideally brittle behavior, using ML as input, the discrepancy between simulated and experimentally tested fracture energy decreases from 37.4% to 12.4%.
- Using the proposed model, the influence of randomized lattice structure on the mechanical properties of cementitious lattices can be also accurately captured. Both in experiment and simulations, the randomized cementitious lattice R5 exhibit similar stiffness to the regular cementitious lattice R0. While, the R5 has 21.6% (22.0% from simulation) lower tensile strength than R0.
- The coefficient α_M regulating bending moment is a critical factor of the lattice model. On the microscale, the α_M determines the tensile strength of local cementitious struts. When $\alpha_M = 0.5$ is used, the simulated tensile strength shows better agreement with experiment. On the macroscale, the α_M doesn't have visible influence on the strength of cementitious lattices, however it determines the post-peak softening behavior and the crack pattern. When $\alpha_M = 0.05$ is adopted, the simulated softening response and crack pattern corresponds with experiment very well.

As mentioned in the introduction, cementitious lattice materials have so far been envisioned for use as lightweight insulation materials (i.e. to work as a substitute of foam concrete in an engineered way). As the

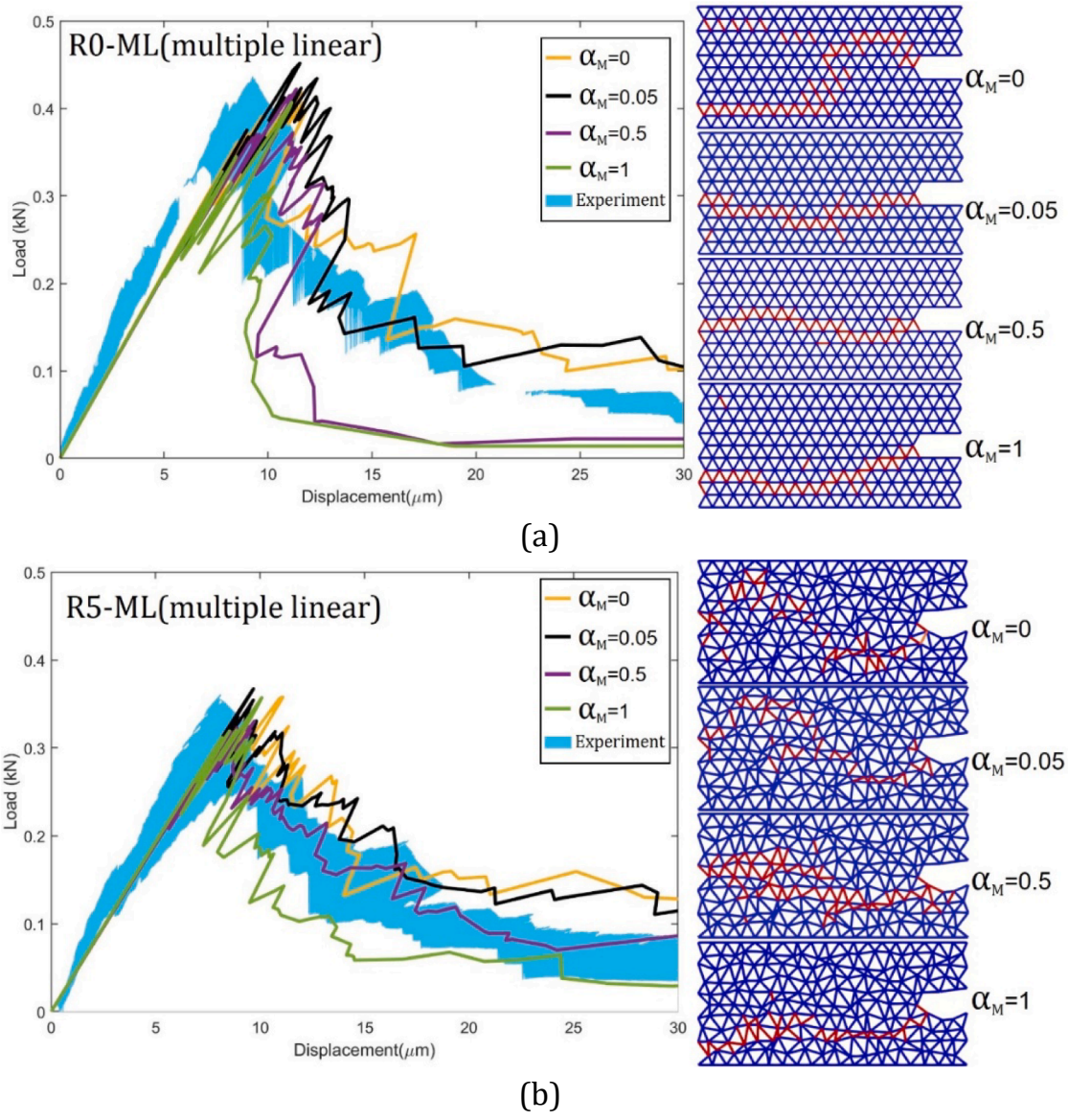

Fig. 22. Smoothed load–displacement simulation curves of macroscopic lattices using different coefficient α_M values, a) R0-ML, b) R5-ML; the crack pattern of cementitious lattices at 30 μm displacement is indicated, failed elements are colored in red.

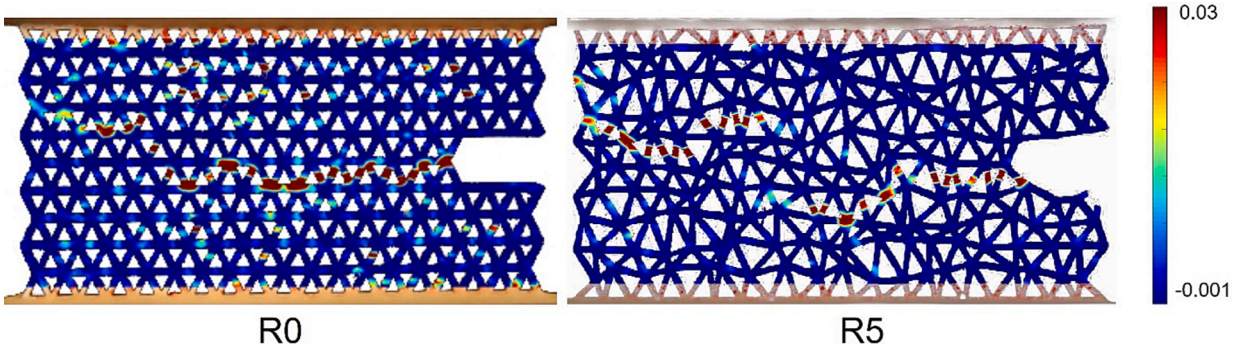

Fig. 23. Crack pattern of the cementitious lattices obtained from DIC.

current study shows, the deformation and fracture behavior of cementitious lattice materials are significantly influence by the heterogeneous microstructure of cement paste and macroscopic lattice structure. More importantly, the proposed modeling method can accurately capture this behavior. In this sense, with the aid of the proposed method one could intentionally introduce heterogeneity, for instance randomness, imperfections and weaknesses, or tailor lattice structure and control the extent of cracking depending on the requirements to tailor crack pattern and fracture resistance of cementitious lattices. The findings of the current study will provide a basis for further research in this direction.

CRediT authorship contribution statement

Yading Xu: Conceptualization, Methodology, Investigation, Formal analysis, Writing – original draft, Visualization. **Yidong Gan:** Writing – review & editing. **Ze Chang:** Writing – review & editing. **Zhi Wan:** Data curation, Writing – review & editing. **Erik Schlangen:** Conceptualization, Writing – review & editing, Supervision. **Branko Šavija:** Writing – review & editing, Supervision.

Declaration of Competing Interest

The authors declare that they have no known competing financial interests or personal relationships that could have appeared to influence the work reported in this paper.

Data availability

Data will be made available on request.

Acknowledgements

Yidong Gan, Ze Chang and Zhi Wan would like to acknowledge the funding supported by China Scholarship Council (CSC) under the grant number 201706130140, 201806060129 and 201906220205.

References

[1] D. Wang, Impact behavior and energy absorption of paper honeycomb sandwich panels, Int. J. Impact Eng. 36 (1) (2009) 110–114.
[2] J.X. Qiao, C.Q. Chen, Impact resistance of uniform and functionally graded auxetic double arrowhead honeycombs, Int. J. Impact Eng. 83 (2015) 47–58.
[3] J.A. Harris, R.E. Winter, G.J. McShane, Impact response of additively manufactured metallic hybrid lattice materials, Int. J. Impact Eng. 104 (2017) 177–191.
[4] J. Liu, et al., On sound insulation of pyramidal lattice sandwich structure, Compos. Struct. 208 (2019) 385–394.
[5] X. Cheng, et al., The equivalent thermal conductivity of lattice core sandwich structure: A predictive model, Appl. Therm. Eng. 93 (2016) 236–243.
[6] K. Wei, et al., Fabrication and heat transfer characteristics of C/SiC pyramidal core lattice sandwich panel, Appl. Therm. Eng. 81 (2015) 10–17.
[7] O.A. Al-Harbi, C. Özgür, M.M. Khan, Fabrication and characterization of single phase cordierite honeycomb monolith with porous wall from natural raw materials as catalyst support, Ceram. Int. 41 (3) (2015) 3526–3532.
[8] Y. Wang, et al., A novel thermally autonomous methanol steam reforming microreactor using SiC honeycomb ceramic as catalyst support for hydrogen production, Int. J. Hydrogen Energy 46 (51) (2021) 25878–25892.
[9] A. Ortona, et al., Cellular ceramics produced by rapid prototyping and replication, Mater. Lett. 80 (2012) 95–98.
[10] J. Bauer, et al., High-strength cellular ceramic composites with 3D microarchitecture, Proc. Natl. Acad. Sci. 111 (7) (2014) 2453–2458.
[11] A. Wang, Yield surfaces of various periodic metal honeycombs at intermediate relative density, Int. J. Plast. 21 (2) (2005) 285–320.
[12] L. Dong, V. Deshpande, H. Wadley, Mechanical response of Ti–6Al–4V octet-truss lattice structures, Int. J. Solids Struct. 60–61 (2015) 107–124.
[13] C. Qiu, et al., Influence of processing conditions on strut structure and compressive properties of cellular lattice structures fabricated by selective laser melting, Mater. Sci. Eng., A 628 (2015) 188–197.
[14] S.Y. Choy, et al., Compressive properties of Ti-6Al-4V lattice structures fabricated by selective laser melting: Design, orientation and density, Addit. Manuf. 16 (2017) 213–224.
[15] Y. Xu, et al., Deformation and fracture of 3D printed disordered lattice materials: Experiments and modeling, Mater. Des. 162 (2019) 143–153.
[16] S.-I. Park, et al., Effective mechanical properties of lattice material fabricated by material extrusion additive manufacturing, Addit. Manuf. 1–4 (2014) 12–23.
[17] M. Lei, et al., 3D printed two-dimensional periodic structures with tailored in-plane dynamic responses and fracture behaviors, Compos. Sci. Technol. 159 (2018) 189–198.
[18] B.G. Compton, J.A. Lewis, 3D-printing of lightweight cellular composites, Adv. Mater. 26 (34) (2014) 5930–5935.
[19] M.S. Pham, et al., Damage-tolerant architected materials inspired by crystal microstructure, Nature 565 (7739) (2019) 305–311.
[20] I. Hager, A. Golonka, R. Putanowicz, 3D Printing of Buildings and Building Components as the Future of Sustainable Construction? Procedia Eng. 151 (2016) 292–299.
[21] Y.W. Tay, et al., Processing and Properties of Construction Materials for 3D Printing, Mater. Sci. Forum 861 (2016) 177–181.
[22] P. Wu, J. Wang, X. Wang, A critical review of the use of 3-D printing in the construction industry, Autom. Constr. 68 (2016) 21–31.
[23] C. Menna, et al., Opportunities and challenges for structural engineering of digitally fabricated concrete, Cem. Concr. Res. 133 (2020), 106079.
[24] P. Aghdasi, et al., An Octet-Truss Engineered Concrete (OTEC) for lightweight structures, Compos. Struct. 207 (2019) 373–384.
[25] L. Li, et al., 3D face-centered-cubic cement-based hybrid composites reinforced by tension-resistant polymeric truss network, Autom. Constr. 120 (2020), 103380.
[26] V. Nguyen-Van, et al., Mechanical performance of fractal-like cementitious lightweight cellular structures: Numerical investigations, Compos. Struct. 269 (2021), 114050.
[27] V. Nguyen-Van, et al., Bioinspired cellular cementitious structures for prefabricated construction: Hybrid design & performance evaluations, Autom. Constr. 119 (2020), 103324.
[28] Z. Wu, Y. Xu, B. Savija, Mechanical Properties of Lightweight Cementitious Cellular Composites Incorporating Micro-Encapsulated Phase Change Material, Materials (Basel) 14 (24) (2021).
[29] Z. Qian, Multiscale Modeling of Fracture Processes in Cementitious Materials. Civil Engineering and Geoscience, TU Delft, Delft, 2012.
[30] H. Zhang, et al., Microscale Testing and Modelling of Cement Paste as Basis for Multi-Scale Modelling, Materials (Basel) 9 (11) (2016).
[31] Y. Xu, et al., Cementitious cellular composites with auxetic behavior, Cem. Concr. Compos. 111 (2020), 103624.
[32] H.S. Wong, N.R. Buenfeld, Determining the water–cement ratio, cement content, water content and degree of hydration of hardened cement paste: Method development and validation on paste samples, Cem. Concr. Res. 39 (10) (2009) 957–965.
[33] E. Schlangen, Crack Development in Concrete, Part 2: Modelling of Fracture Process, Key Eng. Mater. 385–387 (2008) 73–76.
[34] H.S. Wong, M.K. Head, N.R. Buenfeld, Pore segmentation of cement-based materials from backscattered electron images, Cem. Concr. Res. 36 (6) (2006) 1083–1090.
[35] M. Zhang, et al., Computational investigation on mass diffusivity in Portland cement paste based on X-ray computed microtomography (μCT) image, Constr. Build. Mater. 27 (1) (2012) 472–481.
[36] P.D. Tennis, H.M. Jennings, A model for two types of calcium silicate hydrate in the microstructure of Portland cement pastes, Cem. Concr. Res. (2000) 855–863.
[37] C. Hu, Z. Li, Micromechanical investigation of Portland cement paste, Constr. Build. Mater. 71 (2014) 44–52.
[38] Z. Qian, et al., Modeling Framework for Fracture in Multiscale Cement-Based Material Structures, Materials (Basel) 10 (6) (2017).
[39] C.J. Haecker, et al., Modeling the linear elastic properties of Portland cement paste, Cem. Concr. Res. 35 (10) (2005) 1948–1960.
[40] S. Igarashi, M. Kawamura, A. Watanabe, Analysis of cement pastes and mortars by a combination of backscatter-based SEM image analysis and calculations based on the Powers model, Cem. Concr. Compos. 26 (8) (2004) 977–985.
[41] K. Kurumisawa, T. Nawa, Electrical Conductivity and Chloride Ingress in Hardened Cement Paste, J. Adv. Concr. Technol. 14 (3) (2016) 87–94.
[42] J.G. Van Mier, Concrete fracture: a multiscale approach, CRC Press, 2012.
[43] N.E.R. Romijn, N.A. Fleck, The fracture toughness of planar lattices: Imperfection sensitivity, J. Mech. Phys. Solids 55 (12) (2007) 2538–2564.
[44] G. Dong, Y.F. Zhao, Numerical and experimental investigation of the joint stiffness in lattice structures fabricated by additive manufacturing, Int. J. Mech. Sci. 148 (2018) 475–485.
[45] M.H. Luxner, J. Stampfl, H.E. Pettermann, Finite element modeling concepts and linear analyses of 3D regular open cell structures, J. Mater. Sci. 40 (22) (2005) 5859–5866.
[46] J.G. Van Mier, A. Vervuurt, Numerical analysis of interface fracture in concrete using a lattice-type fracutre model, Int. J. Damage Mech. 6 (1997) 408–432.
[47] E. Schlangen, J.G.M.V. Mier, Simple lattice model for numerical simulation of fracture of concrete materials and structures, Mater. Struct. 25 (1992) 534–542.
[48] G. Lilliu, J.G.M.V. Mier, 3D lattice type fracture model for concrete, Eng. Fract. Mech. 70 (2003) 927–941.